Chapter 5

Synaptic Interactions In a Passive Dendritic Tree

Nerve cells are the targets of many thousands of excitatory and inhibitory synapses. An extreme case are the Purkinje cells in the primate cerebellum, receiving between one and two hundred thousand synapses onto dendritic spines from an equal number of parallel fibers (Braitenberg and Atwood, 1958; Llinás and Walton, 1990). In fact, this structure has a crystalline-like quality to it, with each parallel fiber making exactly one synapse onto a spine of a Purkinje cell. For neocortical pyramidal cells, the total number of afferent synapses is about an order of magnitude lower (Larkman, 1991). These number need to be compared against the connectivity in the central processing unit (CPU) of modern computers, where the gate of a typical transistor usually receives input from one, two or three other transistors or connects to one, two or three other transistor gates[1]. The large number of synapses converging onto a single cell provide the nervous system with a rich substratum for implementing a very large class of linear and nonlinear neuronal operations. As we discussed in the introductory chapter, it is only these latter ones, such as multiplication or a threshold operation which are responsible for "computing" in the nontrivial sense of information processing.

It therefore becomes crucial to study the nature of the interaction among two or more synaptic inputs located in the dendritic tree. Here, we restrict ourselves to passive dendritic trees, that is to dendrites that do not contain voltage-dependent membrane conductances. While such an assumption seemed reasonable twenty or even ten years ago, we now know that the dendritic trees of many, if not of most, cells contain significant nonlinearities, including

[1]The reason for this very small *fan-in* and *fan-out* is that each additional gate whose parasitic capacitance needs to be charged up increases the signal propagation delay between consecutive stages, slowing down how fast the clock can operate. Since the clock speed is one of the most important determinants of performance of the final chip, convergence as well as divergence is kept to a minimum. The situation is quite different for random access memory circuits. For example, in a 64 Mbit DRAM (Dynamic Random Access Memory), the fan-in and fan-out associated with the switching transistor at each memory location is approximately 8192. The time taken to charge the large interconnect capacitance that dominates these circuits is reduced through the use of regenerative amplifiers and buffers.

the ability to generate fast or slow all-or-none electrical events, so-called *dendritic spikes*. Indeed, truly passive dendrites may be the exception rather than the rule in the nervous system. We will take up the theme of active dendrites and outline their putative role in computation in chapter 19.

The voltage change in a passive tree in response to two or more current injections is given by the sum of the voltages induced by the individual current inputs. This linearity between current and voltage is expressed in the cable equation 2.7 and is the basis for using input- and transfer impedances to completely charter the behavior of this system. In the absence of any nonlinearity, no true information processing operations can occur. However, as we keep on emphasizing, a synaptic input acts to a change the membrane conductance (in series with a battery), implying that the change in membrane voltage caused by two or more synaptic inputs is **not** the sum of the voltages induced by the individual synaptic inputs. It has not escaped the attention of theoretician that this nonlinearity could be used to implement a type of multiplication (Blomfield, 1974; Srinivasan and Bernard, 1976; Poggio and Torre, 1978, 1981; Torre and Poggio, 1978).

In the following section, we describe the nonlinear interaction between excitation and inhibition which has received particular scrutiny in the literature. In the second part of this chapter, we focus on the multiplicative-like interaction among large number of voltage-dependent NMDA synaptic inputs. The example discussed here is the most plausible instance of a higher-level operation, in this case storing and discriminating complex patterns, implemented using a biophysically very detailed model of a nerve cell. The last section focuses on the important topic of *synaptic microcircuits* (Shepherd, 1972, 1978), that is very small and specific arrangements of synapses between particular neurons. Such microcircuits usually involve so-called dendro-dendritic synapses among two dendrites and are thought to subserve very specific computations.

5.1 Nonlinear Interaction Among Excitation and Inhibition

In section 1.5, we studied this interaction for the membrane patch model. With the addition of the dendritic tree, the nervous system has many more degrees of freedom to make use of and the strength of the interaction depends on the relative spatial positioning as we will see now. That this can be put to good use by the nervous system is shown by the following experimental observation and simple model.

5.1.1 Absolute versus Relative Suppression

For an animal, it is often necessary to completely suppress certain behaviors, while under other conditions the threshold for initiating a behavior should only be elevated but not prevented altogether. Vu and Kranse (1992) study how these two operations can be implemented in the same neuron for the tail-flip escape response in the crayfish. Here, as indeed

in any other animal, during the execution of the escape reflex propelling the animal away from a potential dangerous situation, no additional escape behavior should be initiated. The neuronal influence responsible for this absolute suppression is called recurrent inhibition. While the crayfish is feeding or otherwise engaged, the escape reflex becomes more difficult to initiate. This suppressive influence, termed tonic inhibition, can be overridden in the presence of a strong enough stimulus.

The escape response is mediated by a pair of *lateral giant command* neurons (LG). On the basis of intracellular recordings, Vu and Krasne (1992; see also Vu, Lee and Krasne, 1993) correlate these two types of suppression with distal (tonic inhibition) and proximal (recurrent inhibition) inhibitory inputs onto the dendritic tree of the LG cell (Fig. 5.1B). Since it is know that the excitation mediating the escape reflex is distal from the spike-initiating zone, Vu and his colleagues use the two compartment circuits shown in Fig. 5.1A to model the two forms of inhibition (here by assuming that the GABA-mediated inhibition is of the silent or shunting type with E_i =0). In both cases, excitation is spatially removed from the output of the circuit. For "proximal inhibition", the inhibitory conductance change is located at the output (close to the soma), while for "distal inhibition", excitation and inhibition are both co-localized in the distal compartment. Vu and Krasne point out that in the former case, inhibition always reduces the EPSP by some amount, no matter what the amount of excitation. This, they argue, is the manifestation of *absolute suppression* in the sense that no matter what the excitation, the EPSP—and therefore the behavior—will be suppressed. Quite a different behavior is observed for "distal inhibition:" any amount of inhibition can always be overcome by more excitation, *i.e.* the system demonstrates *relative suppression*. They argue that any behavior that needs to be suppressed no matter what the circumstances should use synaptic inhibition that is close to the soma (*absolute suppression*). Conversely, if the threshold for initiating a behavior needs to be elevated—without abolishing it altogether—distal synaptic inhibition is required.

Let us follow Vu and Krasne (1992) and reduce the neuron to but two compartments, one proximal and one distal to the spike initiation zone. To understand the principle of the spatial interaction we will further assume that the time course of synaptic input is slow compared to the membrane time constant and that inhibition is of the shunting type (*i.e.* E_i =0). Let us first analyze the case when inhibition is proximal, here in the somatic compartment (left side of Fig. 5.1A). Following Kirchhoff's current law that stipulates that the sum of all currents flowing into a node must be zero we can write down for the compartment proximal or close to the spike triggering zone

$$(0 - V_p)g_i + \frac{(0 - V_p)}{R_p} + \frac{(V_d - V_p)}{R_c} = 0\,, \tag{5.1}$$

and for the dendritic compartment

$$(E_e - V_d)g_e + \frac{(0 - V_d)}{R_d} + \frac{(V_p - V_d)}{R_c} = 0\,. \tag{5.2}$$

After a few algebraic manipulations, we arrive at an expression for the proximal depolariza-

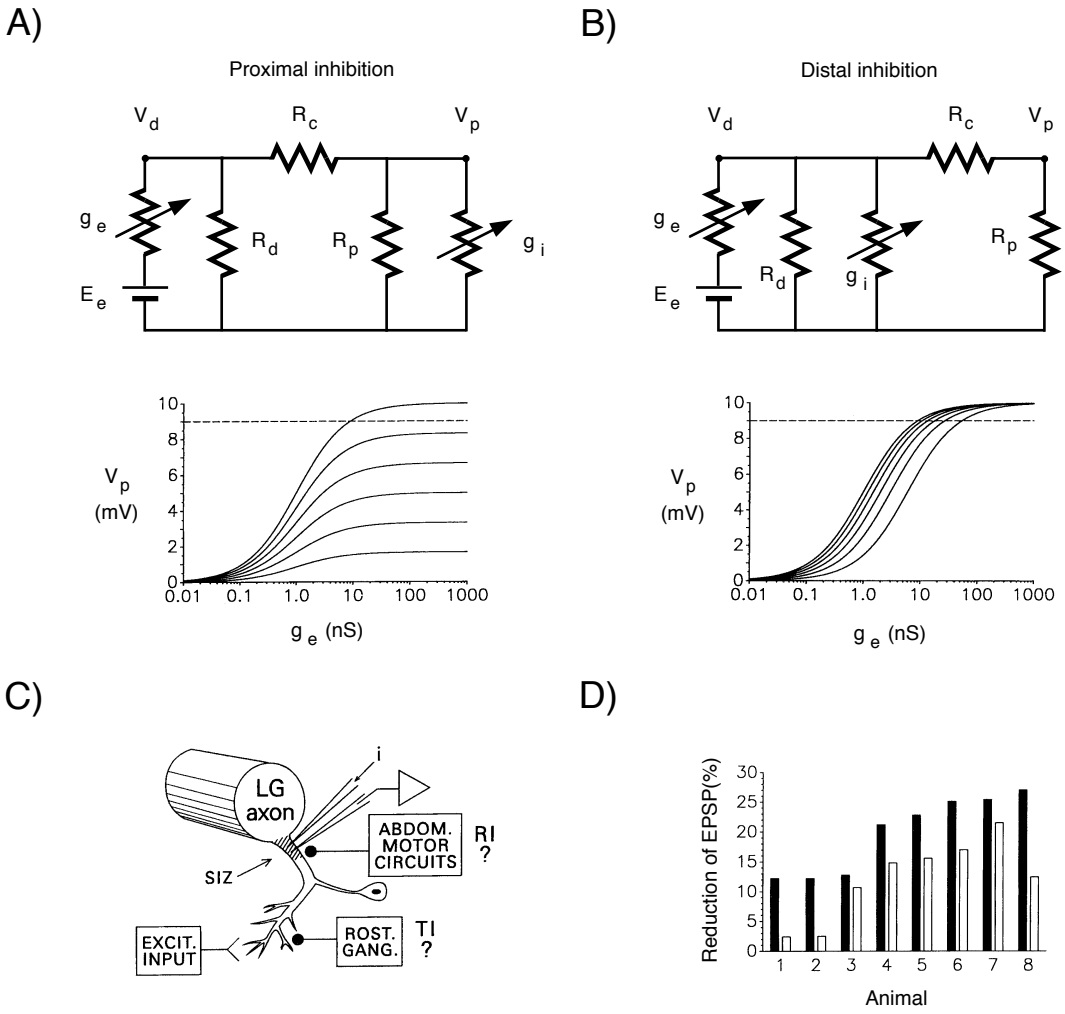

Figure 5.1: Relative versus Absolute Suppression

An important distinction exists between inhibition that can partially suppress an excitatory input (*relative suppression*) versus inhibitory input that can't be overridden by excitation, no matter what its amplitude (*absolute suppression*). These different types of inhibition were demonstrated by Vu and Krasne (1992) in the case of the tail-flip escape behavior in the crayfish. Two circuits that emphasize the relative placement of excitation (with an associated conductance change g_e in series with E_e =100 mV) in the periphery and shunting inhibition (of amplitude g_i and E_i =0) in either the proximal **(A)** or the distal compartment **(B)** (see eqs. 5.3 and 5.5 resp.). The curves were generated using a variable amount of inhibition (0, 0.2, 0.5, 1, 2 and 5 from top to bottom in units of $g_e R_d$). No matter how large the excitatory input, proximal inhibition can reduce the peak potential in a graded manner (*absolute suppression*). This is not true if excitation and inhibition are co-localized, where excitation can always overcome the inhibition, providing a substrate for *relative suppression*. **(C)** Part of the neurobiological circuitry underlying the escape reflex. Excitatory inputs onto the dendrites of the lateral giant command neuron (LG) mediate the reflex. It can be partially suppressed by so-called tonic inhibition (TI), that is inferred to be in the distal dendritic tree. The escape reflex can be completely abolished by recurrent inhibition (RI) that is thought to synapse close to the spike trigger zone. SIZ demarcates the spike initiating zone. **(D)** Another prediction concerns the relative amount of attenuation (the F factor of eq. 5.14) for small (*i.e.* small g_e value; solid bars) and large (large value of g_e; open bars) EPSPs for distal inhibition. The model predicts that smaller EPSPs should be associated with a larger reduction (larger F values) than larger EPSPs, as born out by the data shown here from eight different animals. For proximal inhibition, the F

tion

$$V_p = \frac{E_e g_e R_d R_p}{R_c + R_d + R_p + g_e(R_d R_p + R_d R_c + g_i R_d R_p R_c) + g_i(R_d R_p + R_p R_c)} . \tag{5.3}$$

The amplitude of the EPSP as a function of g_e for various settings of inhibition is plotted in Fig. 5.1A. What is apparent is that a fixed amout of inhibition at the output, *i.e.* the soma, can reduce the EPSP amplitude, no matter what the level of excitation g_e. This absolute dependency on g_i readily becomes apparent in the limit of large excitatory inputs

$$\lim_{g_e \to \infty} V_p = \frac{E_e R_p}{(R_p + R_c + g_i R_c R_p)} . \tag{5.4}$$

Repeating the same analysis for the case that excitation and inhibition are co-localized in the distal compartment leads to

$$V_p = \frac{E_e g_e R_p R_d}{R_c + R_d + R_p + g_e(R_p R_d + R_d R_c) + g_i(R_p R_d + R_d R_c)} . \tag{5.5}$$

Although similar to eq. 5.3, a crucial difference emerges in the limit

$$\lim_{g_e \to \infty} V_p = \frac{E_e R_p}{R_p + R_c} . \tag{5.6}$$

For any fixed level of inhibition, excitation can always override its effect (relative inhibition; right panel in Fig. 5.1A). If excitation and inhibition are not located close to each other, things are different since the local potential saturates at E_e, placing a cap on the amount of current the excitatory input can deliver to the soma. Because of this saturation, inhibition will always be able to reduce the total amount of current delivered to the soma. This would not be true if the synaptic input were to behave as a constant current source, since for $g_e \to \infty$, an infinite amount of depolarizing current would flow to the soma, dominating any loss of current via inhibitory synapses.

5.1.2 General Analysis of Synaptic Interaction in a Passive Tree

Above, we have seen how treating a neuron as more than a single spatial compartment enhances its computational power. Let us now treat the general case of the nonlinear synaptic interaction in a complex dendritic tree using the two-port analysis developed in chapter 3 (Koch *et al.*, 1982).

A word of warning. The theory developed here assumes that the cell operates in its subthreshold domain, where no action potentials are generated. As discussed more fully in chapter 18, modeling the effect of synaptic interaction on a cell's firing rate can yield surprising results quite different from those in the subthreshold domain (Holt and Koch, 1997) and so care must be taken into extending any results without much thought to the suprathreshold domain.

We assume a constant, excitatory input at location e (of amplitude $g_e > 0$ and battery $E_e > 0$) and a constant inhibitory conductance change at location i (of amplitude $g_i > 0$

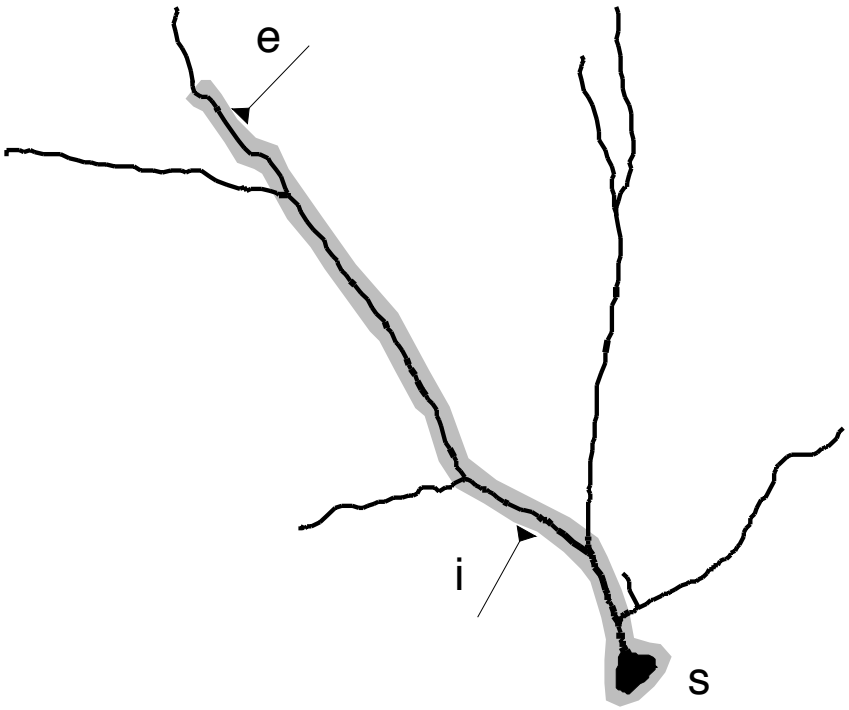

Figure 5.2: INTERACTION AMONG AN EXCITATORY AND AN INHIBITORY SYNAPSE
How does the interaction between an excitatory synapse (at location e) and an inhibitory synapse (at i) in a passive dendritic tree depend on their spatial position? And what role does the synaptic architecture and dendritic morphology play? In general, the potential at the soma (s) is not simply the sum of the individual IPSP and EPSP but can be much less. If the inhibition is of the *shunting* type, with a reversal potential close to the resting potential of the cell, inhibition by itself leads to no significant potential change while still being able to veto the EPSP, as long as the inhibitory synapse is either close to the excitatory one or "on the direct path" between excitation and the soma s (lightly shaded area). The effectiveness of shunting inhibition drops substantially outside this zone.

---

and battery $E_i \leq 0$; see Fig. 5.2). We neglect the time-dependent aspects of this problem, a simplification that allows us to use the input and transfer resistances described in section 3.4, expressing the change in membrane potential as the sum of the currents contributed by the two synapses. At synapse e the synaptic current $I_e = g_e(E_e - V_e)$ will flow, and at location i the current $I_i = g_i(E_i - V_i)$. The composite post-synaptic potential at location e is given by the synaptic current at e multiplied by the input resistance $\tilde{K}_{ee}$ plus the synaptic current at i times the transfer resistance between i and e, $\tilde{K}_{ei}$:

$$V_e = \tilde{K}_{ee} I_e + \tilde{K}_{ei} I_i \,, \tag{5.7}$$

or,

$$V_e = \tilde{K}_{ee} g_e(E_e - V_e) + \tilde{K}_{ei} g_i(E_i - V_i) \,. \tag{5.8}$$

Likewise, for the voltage change at location i we have

$$V_i = \tilde{K}_{ei} g_e (E_e - V_e) + \tilde{K}_{ii} g_i (E_i - V_i)\,, \tag{5.9}$$

where we exploit the symmetry property $\tilde{K}_{ie} = \tilde{K}_{ei}$. Finally, the potential at the soma is given by

$$V_s = \tilde{K}_{es} g_e (E_e - V_e) + \tilde{K}_{is} g_i (E_i - V_i)\,. \tag{5.10}$$

Notice that the voltage is always specified as the product of the appropriate input or transfer resistance and the synaptic current and that the input and transfer resistances are computed in the absence of any synaptic input. Solving these three algebraic equations is straightforward, resulting in the following expression for the somatic potential

$$V_s = \frac{g_e E_e (\tilde{K}_{es} + g_i \tilde{K}_e^+) + g_i E_i (\tilde{K}_{is} + g_e K_i^+)}{1 + g_e \tilde{K}_{ee} + g_i \tilde{K}_{ii} + g_e g_i \tilde{K}^*}\,, \tag{5.11}$$

with

$$\begin{aligned} \tilde{K}_i^+ &= \tilde{K}_{is}\tilde{K}_{ee} - \tilde{K}_{es}\tilde{K}_{ie} \\ \tilde{K}_e^+ &= \tilde{K}_{es}\tilde{K}_{ii} - \tilde{K}_{is}\tilde{K}_{ie} \\ \tilde{K}^* &= \tilde{K}_{ee}\tilde{K}_{ii} - \tilde{K}_{ie}^2\,. \end{aligned}$$

Whether or not the somatic potential is positive or negative, that is whether it corresponds to an EPSP or to an IPSP, depends on the relative magnitude of the two contributions.

In order to arrive at a qualitative picture of the behavior of the system, let us assume that the conductance inputs g_e and g_i are small, such that $g_e \tilde{K}_{ee} \ll 1, g_i \tilde{K}_{ii} \ll 1$, and $g_e g_i K^* \ll 1$, and that higher than second-order terms in g_e and g_i can be neglected (e.g., $g_e^3 \approx 0$ and $g_e g_i^2 \approx 0$, etc.). Similarly to eq. 4.14, we can use the Taylor series expansion of eq. 5.11 to arrive at

$$\begin{aligned} V_s &\approx \tilde{K}_{es}\,[g_e E_e - g_e \tilde{K}_{ee}(g_e E_e) - g_e \tilde{K}_{ie}(g_i E_i)] \\ &\quad + \tilde{K}_{is}\,[g_i E_i - g_i \tilde{K}_{ii}(g_i E_i)\ - g_i \tilde{K}_{ie}(g_e E_e)] \\ &\approx \tilde{K}_{es}[I_e + I_{ee} + I_{ei}] + \tilde{K}_{is}[I_i + I_{ii} + I_{ie}]\,. \end{aligned} \tag{5.12}$$

The three components in the first bracket are a short-hand version of the currents flowing at locations e that are propagated to the cell body, and the three currents in the second bracket are propagated from the site of inhibition to the soma. I_e is the current generated under the assumption that the driving potential remains unperturbed (*i.e.* $E_e - V_e \approx E_e$). I_{ee} "corrects" the first term by approximating the driving potential as the difference between E_e and the voltage change $\tilde{K}_{ee} g_e E_e$ associated with the first term. I_{ei} results from the interaction between the two synapses. It can be interpreted as follows: the first-order approximation to the inhibitory current is $g_i E_i$, causing an IPSP at e of amplitude $\tilde{K}_{ie} g_i E_i$ which will affect the driving potential at e. The appropriate correction current is given by the IPSP multiplied by the local conductance change $-g_e \tilde{K}_{ie} g_i E_i$. By analogy, the currents at the site of the inhibition can likewise be explained by the superposition of a zero-order current plus the first two correction currents.

5.1.3 Location of the Inhibitory Synapse

So far, we did not discuss any specific spatial arrangements between excitation and inhibition. We are interested in finding the location where synaptic inhibition can be maximally effective in reducing the amplitude of the excitatory input. Specifically, given an excitatory synapse (of amplitude g_e and battery E_e) at location e, where should the inhibitory synapse (of amplitude g_i and battery E_i) be located such that it maximally reduces the EPSP? This question was the subject of an investigation into the relationship between synaptic architecture and dendritic morphology (Koch *et al.*, 1982, 1983). It is tedious, but straightforward (Koch, 1982) to prove the following:

> **On-the-path theorem.** *For arbitrary values of* $g_e > 0, g_i > 0$, $E_e > 0$ *and* $E_i \leq 0$, *the location where inhibition is maximally effective is always on the direct path from the location of the excitatory synapse to the soma (Fig. 5.2).*

Where exactly the optimal location is on this path depends on the details of the system and can shift from the location of the excitatory synapse to somewhere on the path to the cell body. As inhibition is moved towards the soma, its specificity decreases, since the same inhibition now not only reduces the EPSP coming from synapse e but also the EPSPs from pther locations. This is most pronounced at the soma, where an excitatory input anywhere in the dendritic tree will be attenuated. Thus, mapping synaptic architecture onto the dendritic morphology can give rise to different classes of computations.

Three useful properties concerning the optimal location of inhibition (see also Jack *et al.*, 1975; Rall, 1967, 1970) that are valid for stationary conductance inputs in arbitrary, passive dendritic trees are:

(i) For small synaptic inputs g_e and g_i, the most relevant parameter is the distance between the two synapses. It makes only little difference whether inhibition is behind (with respect to the cell body) excitation or on the path. The strength of the interaction among synapses decreases as the amplitudes of the conductance changes are decreased.

(ii) As g_e increases while g_i remains constant, the optimal location of inhibition moves along the direct path towards the soma.

(iii) For very large excitatory inputs ($g_e \to \infty$), all inhibitory synapses located behind the excitatory synapse are completely ineffective.

These properties are a direct consequence of eq. 5.11, the fact that there exists an unique path between any two points in a dendritic tree, and properties of the transfer resistances (section 3.4).

Experimental verification of the specific nature of synaptic inhibition comes from a study by Skydsgaard and Hounsgaard (1994) carried out on the large dendritic arbor of motoneurons. Using three independent electrodes that can release either glutamate or GABA (so-called *iontophoresis* electrodes) as well as a fourth recording electrode at the cell body, they

showed in ten out of twelve experiments a spatially specific reduction in the glutamate-induced excitatory response. In other words, the shunting action of GABA was primarily effective in reducing the excitatory action of glutamate when the two iontophoresis electrodes were close to each other. No or little effect was observed on the response due to a more distal glutamate-releasing electrode. This constitutes *prima facie* evidence for the spatial selectivity of shunting inhibition.

5.1.4 Shunting Inhibition Implements a "Dirty" Multiplication

Let us consider the specific case when inhibition has a reversal potential close or equal to the resting potential of the cell. The $GABA_A$ mediated increase in chloride conductance approximates such a *shunting* inhibition. In this case, the nonlinear interaction between excitation and inhibition is the most pronounced, because activation of silent inhibition by itself does not cause any change in potential (hence its proper—but rarely used—name of *silent* inhibition), while inhibition during synaptic excitation can greatly reduce the EPSP. For small enough inputs eq. 5.11 reduces to

$$V_s \approx E_e \left[g_e \tilde{K}_{es} - g_e^2 \tilde{K}_{ee} \tilde{K}_{es} - g_e g_i \tilde{K}_{ei} \tilde{K}_{is} \right]. \tag{5.13}$$

Here the somatic potential is given by two terms in g_e in addition to a cross-term involving a multiplicative interaction between g_e and g_i. Conceptually, one can think of this as a *dirty* or *approximate multiplication* between two synaptic inputs g_e and g_i, with the value of the offset $(g_e \tilde{K}_{es} - g_e^2 \tilde{K}_{ee} \tilde{K}_{es})$ depending in a nonlinear manner on one of the inputs (Poggio and Torre, 1978).

In order to quantify the effectiveness of shunting inhibition, Koch and colleagues (1982) introduced the F factor as the ratio of the somatic EPSP in the absence of any inhibition to the somatic EPSP in the presence of inhibition; the larger this number the stronger the effect of inhibition. On the basis of eq. 5.11 this can be expressed as

$$F = \frac{g_e \tilde{K}_{es}}{1 + g_e \tilde{K}_{ee}} \cdot \frac{1 + g_e \tilde{K}_{ee} + g_i \tilde{K}_{ii} + g_e g_i \tilde{K}^*}{g_e \tilde{K}_{es} + g_e g_i \tilde{K}_e^+}, \tag{5.14}$$

where $\tilde{K}_e^+ = 0$ for inhibition located on the path between e and s. A large F value describes an effective inhibition, $1/F$ indicating the relative decrease of the somatic EPSP by inhibition. As expected, $F \geq 1$ for all cases. Table 5.1 illustrates some typical F values obtained in a numerical simulation of the effect of inhibition in a retinal ganglion cell responding to a single excitatory input at location 1 (Fig. 5.3A). Let us summarize these results.

The Effectiveness of Shunting Inhibition

(i) For small synaptic inputs the on-the-path effect is weak and the strength of the interaction depends mainly on the distance between excitation and inhibition. Under these conditions, all locations close to the excitatory synapse are equally effective in reducing excitation.

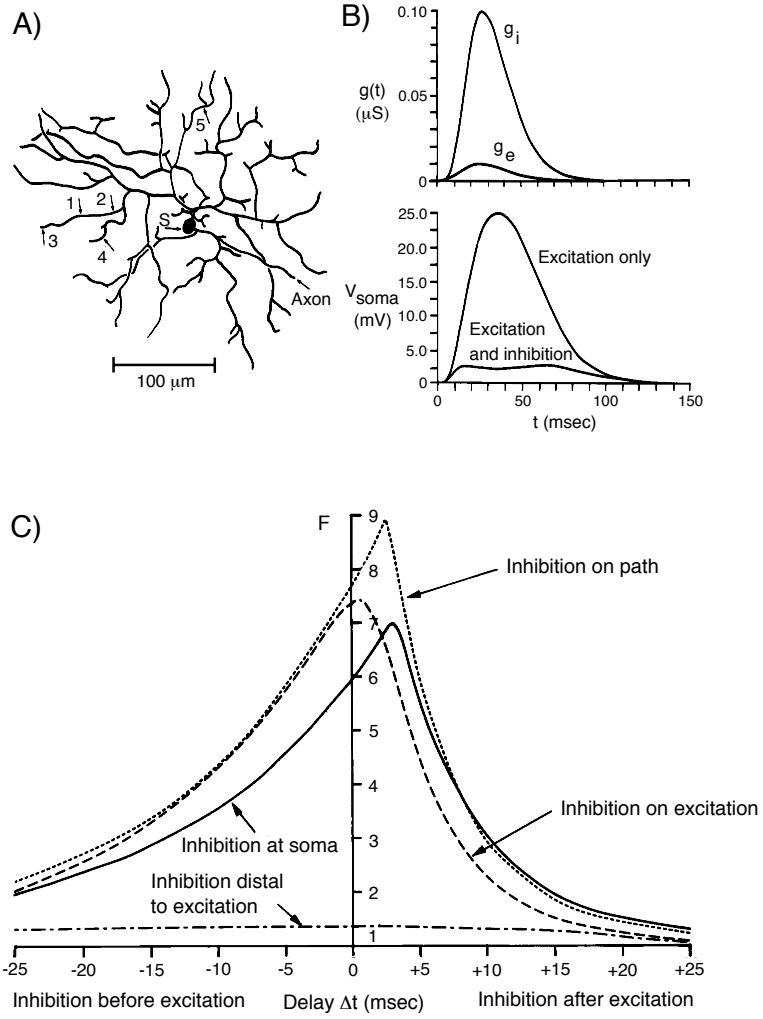

Figure 5.3: Spatio-Temporal Specificity of Synaptic Interaction
The effectiveness of shunting inhibition ($E_i = V_{rest}$) in vetoing an EPSP in a retinal ganglion cell. **(A)** Excitation is always at location 1, while the position of the inhibitory synapse varies. The cell's morphology was reconstructed based on Golgi material from Wässle, Illing, and Peichl (1979). **(B)** The time-course of the excitatory and the inhibitory conductance changes reflect the slow retinal dynamics (Baylor and Fettiplace, 1979), with identical time courses but different peak conductance changes (10 nS for excitation and 100 nS for inhibition). **(C)** The F factor, *i.e.* the reduction in the peak somatic EPSP due to inhibition, as a function of the delay between the onset of $g_e(t)$ and $g_i(t)$. The strength of the interaction (see also Table 5.1), is specific in space and in time. This result holds over a large parameter range. In particular, R_m (here set to 14,000 Ωcm^2) can be increased over several orders of magnitude. From Koch *et al.* (1983).

(ii) If the two synapses coincide anywhere in the dendritic tree ($i = e$), F reduces to

$$F = 1 + \frac{g_i \tilde{K}_{ii}}{1 + g_e \tilde{K}_{ii}}. \tag{5.15}$$

Inhibition at location	g_e 1 / g_i 1	1 / 10	1 / 100	10 / 100
3	1.16	2.06	3.43	1.96
1	1.17	2.70	1.80	7.72
2	1.14	2.40	15.00	8.72
4	1.12	1.72	2.47	1.87
5	1.08	1.46	1.84	1.62
s	1.11	2.06	11.57	9.18

Table 5.1: EFFECTIVENESS OF SHUNTING INHIBITION

F values, describing the effectiveness of shunting inhibition in reducing a somatic EPSP, for stationary synaptic inputs in the retinal ganglion cell of Fig. 5.3A. The excitatory synaptic input g_e (with E_e =80 mV relative to V_{rest}) is always at location 1, while inhibition g_i is either located behind excitation (3), at the same location as excitation (1), between excitation and the soma (2), in an branch just off the path (4), in a very different part of the tree (5) or at the soma (s). The amplitude of g_e and g_i are in nS. The somatic EPSP in the absence of any inhibition for g_e =1 nS is 6.56 mV. $R_m = 14,000\ \Omega cm^2$ and $R_i = 70\ \Omega cm$. From Koch (1982).

This is also the F factor obtained when dealing with a patch of passive membrane in the presence of two synapses (if we identify R with $\tilde{K}_{ii}$). The difference between eqs. 5.14 and 1.34 (or 5.15) is due spatially distributed tree. As discussed in section 5.1.1, excitation can always overcome the effect of fixed but large inhibition.

(iii) If the amplitude of inhibition is above a critical value (about 50 nS in the case of the retinal ganglion cell simulation; Koch *et al.*, 1983), F values can be quite high (2-8), even if the excitatory input is much larger than the inhibitory one, as long as the inhibition is between excitation and the soma. Comparing this against the F factor obtained in a lumped circuit model (eq. 5.15), we ascertain that these high F values are due to the cable properties of the tree. Inhibition behind excitation or on a neighboring branch (about 10 or 20 μm for the retinal ganglion cell considered here) off the direct path is ineffective in reducing excitation significantly.

(iv) The specificity for high values of g_i persists even for very large values of the membrane resistivity, when the cell is relatively compact (in terms of electrotonic distance or in terms of the logarithm of the voltage attenuation L^v). For instance, for R_m = 1 $M\Omega cm^2$, the electrotonic size of the ganglion cell in Fig. 5.3A shrinks to 0.03λ and its input resistances increase to over 1 GΩ. Yet for g_e =10 nS and g_i =100 nS, we obtain F =10.5, 14.5, 21.0, 2.4, 2.7 and 2.7 for inhibition at the location of excitation (1), on-the-path (2), at the cell body (s), behind excitation (3), on a neighbouring branch (4) and in a different part of the tree (location 5; see Fig. 5.3A). These strong

effects can be visualized by recalling our loose analogy between dendrites and water pipes and reservoirs. Shunting inhibition corresponds to opening a hole in the pipe, coupled to a water reservoir with the same pressure as in the quiescent pipe system. If this hole is between the site where water is being injected and the central pool it is clear that more water will leave the hole on its way to the large somatic sink than if the hole were to be opened upstream from excitation.

We conclude that if g_i is large enough, the on-the-path condition becomes very specific such that blocking an EPSP is only possible if inhibition is either in the close neighborhood of the excitatory synapse or between excitation and the cell body. Rall (1964) observed earlier that in a single unbranched cable, shunting inhibition effectively vetoes more distal but not more proximal excitation.

Temporal Specificity

So far we only considered the case of stationary synaptic inputs. In the general time-dependent case, the algebraic eqs. 5.8-5.10 are replaced by integral equations

$$\begin{aligned} V_e(t) &= (g_e(t)[E_e - V_e(t)]) * K_{ee}(t) + (g_i(t)[E_i - V_i(t)]) * K_{ei}(t) \\ V_i(t) &= (g_e(t)[E_e - V_e(t)]) * K_{ei}(t) + (g_i(t)[E_i - V_i(t)]]) * K_{ii}(t) \\ V_s(t) &= (g_e(t)[E_e - V_e(t)]) * K_{es}(t) + (g_i(t)[E_i - V_i(t)]) * K_{is}(t)\,. \end{aligned} \tag{5.16}$$

Typically, these equations are solved numerically (Segev and Parnas, 1983; Koch *et al.*, 1983). The efficacy of inhibition is characterized by a slight generalization of the F factor of eq. 5.14 (F is defined as the ratio of the peak amplitude of the somatic EPSP without inhibition to the peak of the somatic EPSP in the presence of inhibition).

Fig 5.3 shows the dependency of F on the relative timing between the onset of excitation and inhibition. Negative delays correspond to inhibition preceding excitation, while positive delays are associated with inhibition following excitation. As can be seen, the specificity of shunting inhibition in vetoing EPSPs generalizes from space to time: on-the-path inhibition can effectively veto excitation if it occurs within about 10 msec of the onset of excitation, about two-thirds of the membrane time constant. As we discussed in section 3.6, the local delay D_{ii} (Agmon-Snir and Segev, 1993) specifies the window during which synaptic inputs can interact with each other. Different locations have different temporal windows associated with them (e.g. Fig. 3.12), allowing for an operationalized definition of what is meant by two *simultaneous* inputs.

The delay between the onset of excitation and optimal inhibition increases with increasing distance between the two synapses, as expected from the definition of the propagation delay oin eq. 2.51.

Decreasing the duration of inhibition below that of excitation decreases its effectiveness, in some cases dramatically. In no case did the F factor for transient inputs exceed the F factor for the corresponding stationary case. That is, inhibition appears to be at it most effective if temporal effects can be discounted.

Fig. 5.3 demonstrates the on-the-path effect very vividly. Locating inhibition between the site of the excitatory synapse and the soma can shunt the somatic EPSP by a maximal factor of 9, while moving inhibition beyond excitation (approximately conserving the distance between the two synapses) renders inhibition much less effective, with the F factor dropping to 1.3 (a reduction of about 7). Yet this specificity only occurs in the presence of large conductance changes, possibly outside the physiological range (see Table 5.1) and becomes much less pronounced for smaller values of g_i, when the interaction depends more on the distance between excitation and inhibition.

In summary, the veto effect of inhibition can be strong and specific with respect to spatial location and relative timing provided the following requirements are fulfilled: (i) inhibition must have a reversal potential close to the resting potential of the cell, (ii) inhibition should be close to excitation or on the direct path between excitation and the cell body, (iii) peak inhibition must be large enough and (iv) inhibition must last (at least) as long as excitation and their time courses should overlap substantially.

5.1.5 Hyperpolarizing Inhibition Acts Like a Linear Subtraction

As we saw above, in the limit of small synaptic inputs ($g_e\tilde{K}_{ee} \ll 1$ and $g_i\tilde{K}_{ii} \ll 1$), the action of shunting inhibition on excitation can be characterized as a multiplication with an offset. Even though the interaction between hyperpolarizing inhibition, such as the $GABA_B$ complex that increases the postsynaptic potassium conductance (reversing close to -100 mV), and excitation also contains such multiplicative effects, it is more linear due to the direct contribution the hyperpolarizing battery makes toward the membrane potential. Inspection of eq. 5.12 reveals that the first two terms in $\tilde{K}_{is}$ are proportional to the reversal potential of the inhibitory synapses. The more negative the inhibitory reversal potential (relative to V_{rest}), the more these terms will dominate and the more the overall operation will resemble a linear subtraction.

A physiological instance of such a subtractive inhibition that can be linked to a specific computation occurs in the fly's *motion detection system*. Hassenstein and Reichardt (1956; Reichardt, 1961) first suggested that the key mechanism underlying the optomotor response of insects to moving stimuli is mediated by a correlation-like operation. In this scheme, the output from one receptor is multiplied by the temporally delayed (e.g. low-pass filtered) output from a neighbouring receptor and then temporally averaged. The component that is direction selective can be extracted from the component that is independent of the direction of motion by subtracting the output of two, mirror-symmetric pairs of Reichardt detectors from each other.

A computational analysis (Egelhaaf, Borst and Reichardt, 1989) of this system predicts that as the subtraction stage between opposite oriented motion detectors is blocked, the power of the second-order component of the membrane potential in the cellular output stage increases. Experiments with picrotoxin, a blocker of $GABA_A$ receptors confirm this (Egelhaaf, Borst and Pilz, 1990). Intracellular recordings from large tangential cells in the lobula plate in the blowfly in combination with pharmacological blockers show that the

excitatory input is mediated by fast cholinergic synapses while the subtraction relies on GABAergic synapses that reverse around -75 mV (Borst, Egelhaaf and Haag, 1995; Brotz and Borst, 1996). A stable resting potential around -50 mV (Fig. 5.4) gives the membrane enough manovering room in both directions to implement a linear operation of importance to optomotor behavior in flies.

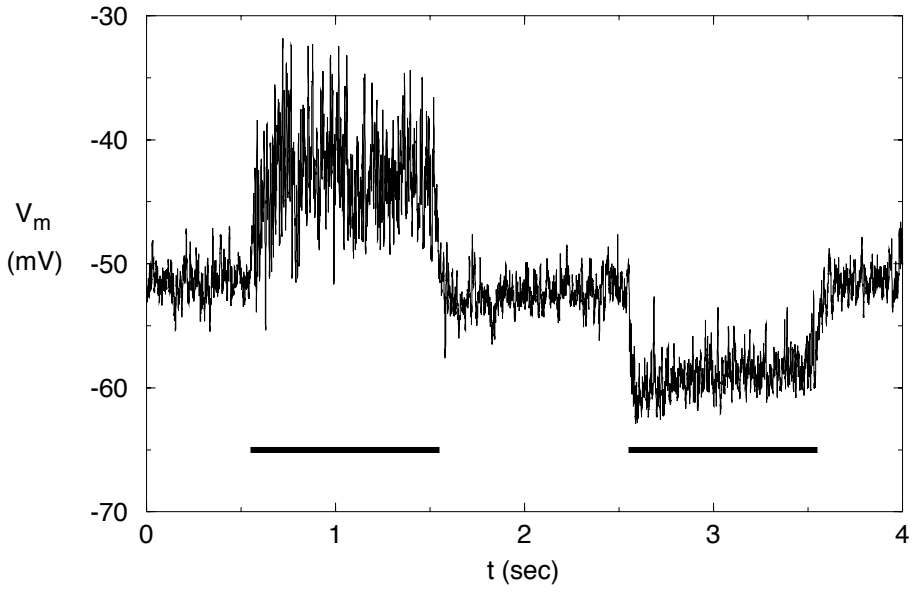

Figure 5.4: Linear Subtraction in the Motion Pathway of the Fly
Intracellular recording from a VS cell in the third optic ganglion of the blowfly *Calliphora* during motion of a whole-field grating. This stimulus is moved for one second in the preferred (first black bar) and for one second in the cell's opposite, or null, direction (second black bar) past the fly. The resting potential is stable around -50 mV, explaining the more-or-less symmetric response pattern driven by opposing pairs of Reichardt correlation detectors (Borst, Egelhaaf and Haag, 1995). Excitation is mediated by fast cholinergic and inhibition by GABAergic synaptic input onto this cell. Unpublished data from J. Haag and A. Borst.

5.1.6 A Functional Interpretation of the Synaptic Architecture and Dendritic Morphology: AND-NOT Gates

The specificity of the interaction between excitation and shunting or silent inhibition provides *in principle* the substrate for implementing different classes of analog computations in different dendritic trees. This situation is portrayed in a highly idealized but suggestive manner in Fig. 5.5 using a logical metaphor (Koch *et al.*, 1982), bearing in mind that these interactions are continuous and not all-or-none.

In an unbranched cable (Fig. 5.5A), input i_1 can inhibit more distal excitatory input e_1, e_2 and e_3, while inhibition i_3 can only significantly affect e_3. If we adopt the logical

AND-NOT all-or-none operation to characterize this interaction (an output only occurs in the presence of excitation *and no* inhibition), such a cable implements the logical expression

$$[e_3 \text{ AND} - \text{NOT } (i_1 \text{ OR } i_2 \text{ OR } i_3)] \text{ OR}$$
$$e_2 \text{ AND} - \text{NOT } (i_1 \text{ OR } i_2) \text{ OR } (e_1 \text{ AND} - \text{NOT } i_1)\,. \tag{5.17}$$

In other words, the soma receives a significant signal only if e_3 is high and not blocked by i_1, i_2 or i_3, or if e_2 is high and not vetoed by either i_1 or i_2, or if e_1 is high and not vetoed by i_1. Due to the on-the-path effect, the more branched dendritic tree in Fig. 5.5B implements a different expression,

$$(e_1 \text{ AND} - \text{NOT } i_1) \text{ OR } (e_2 \text{ AND} - \text{NOT } i_2) \text{ OR } \{[(\, e_3 \text{ AND} - \text{NOT } i_3) \text{ OR}$$
$$(e_4 \text{ AND} - \text{NOT } i_4) \text{ OR } (e_5 \text{ AND} - \text{NOT } i_5) \text{ OR } (e_6 \text{ AND} - \text{NOT } i_6)] \text{ AND} - \text{NOT } i_7\} \tag{5.18}$$

Thus, the combination of dendritic morphology coupled with specific synaptic circuits conspires to create a rich class of nonlinear operations, with different dendritic trees carrying out different computations. These interactions would be based on voltage-independent AMPA excitatory synapses and GABA_A inhibitory synapses.

The "dendritic-tree-as-logic-network" metaphor has been a popular concept that has been extended to a number of other biophysical situations and logical operators (Segev and Rall, 1988; Shepherd and Brayton, 1987; Shepherd, 1990; Zador, Claiborne and Brown, 1992; see chapters 12 and 19).

Yet as succinctly summarized by Mel (1994), this simile can be criticized on several grounds. The principal argument against postulating that specific arrangements of individual synapses act as logical or analog gates is the great demand that this places on developmental processes. In order to achieve the precise type of wiring idealized in Fig. 5.5, some learning mechanism has to guide individual synapses to individual branches in the dendritic tree to achieve the precise spatial arrangements required. For instance, moving i_7 in Fig. 5.5B to the adjacent branch significantly changes the associated logical expression. Thus, the great specificity of this interaction represents at the same time its own Achilles heel (Mel, 1994).

It is possible, of course, that on-the-path effects are exerted not by individual synaptic inputs but by groups of synapses as is the case in the distinction between absolute and relative suppression (Vu and Krasne, 1992). This spatially less precise degree of spatial interactions places a much reduced burden on developmental processes, since it only specifies that inhibitory synapses should either be adjacent to the excitatory ones or in a different part of the dendritic tree.

On biophysical grounds, it is unclear how specific the interaction for between excitatory and inhibitory synapses actually is. As illustrated in Table 5.1, if the amplitude of the inhibitory conductance change is small, little specificity results. Furthermore, during physiological conditions, the cell potential may never be at V_{rest} because the cell receives tonic excitatory input. Under these conditions, the distinction between hyperpolarizing and shunting inhibition is much smaller than we assume here, since both reverse negative to the "effective" resting potential.

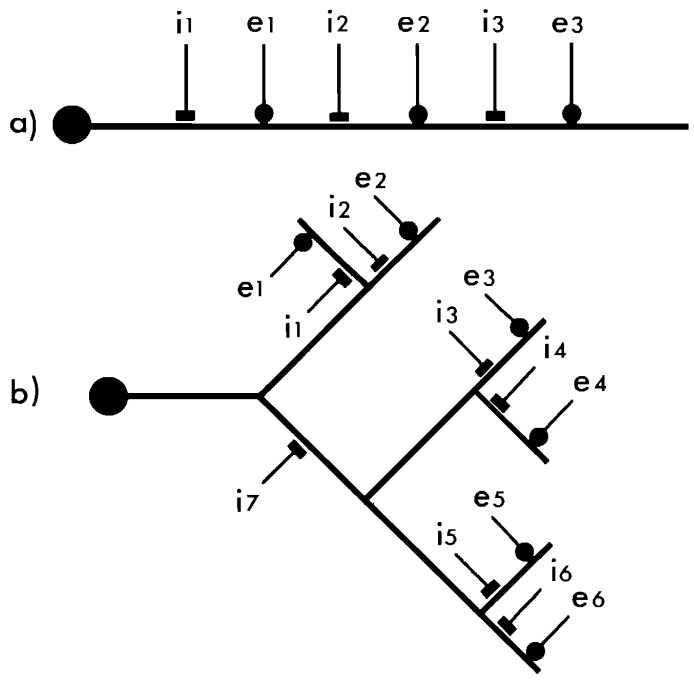

Figure 5.5: Implementing AND-NOT Logic in a Dendritic Tree
An idealized, binary view of the continuous nonlinear interactions occurring between excitation and shunting inhibition. Inhibitory inputs (rectangles) veto more distal excitatory inputs (circles), but have only a marginal effect on inputs more proximal to the soma, thereby approximating a logical AND-NOT gate. The two distinct dendritic architectures, coupled with specific synaptic wiring, implement very different logical expressions (see the expressions 5.17 and 5.18). From Koch *et al.*, (1982).

5.1.7 Retinal Directional Selectivity and Synaptic Logic

Direction selectivity of retinal ganglion cells is one example of a complex nonlinear operation that appears to use synaptic logic (Koch, Poggio and Torre, 1986). A subset of ganglion cells in the vertebrate retina fire vigorously in response to motion of a spot of light in one direction, the preferred one, but are silent to motion in the opposite, the null direction. The classical experiments of Barlow and Levick (1965) inferred that synaptic inhibition—now known to be GABAergic—plays a critical role, by preventing the cell to respond in the null direction. More recent work on rabbit ganglion cells reveals an additional facilitatory direction-selective component (Grzywacz and Amthor, 1993).

A popular model for the biophysical basis of direction-selectivity is nonlinear synaptic interaction between cholinergic excitation and GABAergic inhibition mediated by $GABA_A$ receptors in the dendritic tree of ganglion cells (Torre and Poggio, 1978; Koch *et al.*, 1982, 1983, 1986). Intracellular recordings from turtle and fog direction-selective ganglion cells support activation of shunting inhibition in the null direction (Marchiafava, 1979; Watanabe

and Murakami, 1984). The very complex dendritic morphology of direction-selective ganglion cells (Oyster, Amthor and Takahashi, 1993) provides an ideal substrate for numerous local and nonlinear veto-operations of the type schematized in Fig. 5.5B.

Yet in some ganglion cells, direction selectivity is maintained or even reversed in the presence of pharmacological blockers of GABA. Patch-clamping the dendrites of turtle ganglion cells revealed an excitatory input that is already direction-selective (Borg-Graham, 1991b). Furthermore, motion in the preferred direction causes a much larger increase in the input conductance that null direction motion, in conflict with the models presented here in which the exact temporal relationship between excitation and inhibition shapes the postsynaptic response but the total conductance change remains invariant to the direction of motion (e.g. Fig. 5.3).

It thus appears that at least some fraction of the direction-selective response is computed presynaptically, most likely in cholinergic neurons possessing a unique dendritic branching pattern called *starburst amacrine* cells (Masland, Mills and Cassidy, 1984). In the rabbit, starburst amacrine cells are well situated to provide synaptic input from their distal dendrites to directionally-selective ganglion cells via graded, dendro-dendritic synapses (Vaney, Collin and Young, 1989). Their distinctive dendritic branching pattern is especially suited for local generation of directionally-selective outputs, such that direction-selectivity could be implemented using a combination of nonlinear synaptic interaction and inhibitory kinetics that are slower than that for excitation (Borg-Graham and Grzywacz, 1992). In the second scheme, excitation is always trailed by a slower inhibitory wave—if the activated synaptic input is moving *towards* a site of synaptic output (in this case a dendritic tip) excitation reaches the output before the inhibtion catches up. On the other hand, if the input is moving *away* from the output the inhibition, interposed between the excitation and the output, effectively shunts the excitatory current, preventing it from depolarizing the output zone (see also Rall, 1964). Yet, biophysical simulations of amacrine cells suggest that the non-linear interaction of excitation and inhibition probably is the dominant mechanism generating a directional selective response under normal conditions (Borg-Graham and Grzywacz, 1992).

The final verdict is not in. It appears likely that even such a simple operation as distinguishing the direction of a moving stimulus is implemented using a plurality of biophysical mechanisms acting at several sites, some requiring inhibition and some not (Amthor and Grzywacz, 1993). Such redundancy might be necessary in the face of demands that the circuitry wire itself up during development and retain its specificity in the face of a constantly varying environment.

5.2 Nonlinear Interaction Among Excitatory Synapses

What about the interaction expected between two excitatory (with synaptic reversal potential E_e and stationary conductance increases g_1 and g_2) voltage-independent synaptic input?

If both synapses are co-localized, the somatic EPSP will be of amplitude

$$\frac{(g_1+g_2)E_e\tilde{K}_{es}}{1+(g_1+g_2)\tilde{K}_{ee}} = \frac{g_1E_e\tilde{K}_{es}}{1+(g_1+g_2)\tilde{K}_{ee}} + \frac{g_2E_e\tilde{K}_{es}}{1+(g_1+g_2)\tilde{K}_{ee}}\,. \tag{5.19}$$

In the opposite case, when two sites 1 and 2 are electrotonically decoupled, *i.e.* $\tilde{K}_{12} \to 0$, the somatic potential is given by

$$\frac{g_1E_e\tilde{K}_{1s}}{1+g_1\tilde{K}_{11}} + \frac{g_2E_e\tilde{K}_{2s}}{1+g_2\tilde{K}_{22}}. \tag{5.20}$$

Assuming that $\tilde{K}_{ee} \approx \tilde{K}_{11} \approx \tilde{K}_{22}$ and $\tilde{K}_{es} \approx \tilde{K}_{1s} \approx \tilde{K}_{2s}$ (*i.e.* 1 and 2 have the same electrotonic properties), it is clear that the somatic EPSP is smaller if both synapses coincide (eq. 5.19) then if both are far apart (eq. 5.20). The same results holds true even if the coupling term $\tilde{K}_{12}$ is non-zero and transient inputs are considered (Koch *et al.*, 1982). The reason for this *sublinear addition* is simply the fact that as the postsynaptic potential increases, the amount of current flowing through voltage-independent excitatory synaptic channels decreases (Rall, 1977).

Experimental studies of these predictions have been scant, with the large motoneurons providing a favorite preparation. Two earlier studies (Burke, 1967; Kuno and Miyahara, 1969) had concluded, based on an indirect inferrence, that excitatory inputs interacts sublinearly when located somewhere in the distal dendritic tree. In the above mentioned Skydsgaard and Hounsgaard (1994) experiment, glutamate was locally applied to different parts of the dendritic tree of turtle motoneurons from two independent iontophoresis electrodes. At the cell's resting potential they observed linear summation at the soma (see also Langmoen and Andersen, 1983) which turned supralinear as the membrane was depolarized by the recording electrode (most likely due to amplifying voltage-dependent membrane conductances). Yet basic biophysics implies nonlinear saturation due to the conductance-increasing nature of synaptic input. Is it possible that synaptic saturation is always compensated for by voltage-dependent outward currents distributed in the dendritic tree? And if so, why?

5.2.1 Sensitivity of Synaptic Input to Spatial Clustering

As emphasized in chapter 4, in the central nervous system many, if not most, neurons receive synaptic input from a mixture of voltage-independent AMPA and voltage-dependent NMDA ionotrophic synapses.

For instance, a major role for NMDA input in cat visual cortex is supported by experiments that blocked NMDA responses using the pharmacological agent APV. This procedure caused the visual response of neurons whose cell bodies are located in the upper three layers to be either strongly attenuated or eliminated altogether, while neurons in the input layer 4 could still be visual activated (Miller, Chapman and Stryker, 1989; Fox, Sato and Daw, 1990; Daw, Stein and Fox, 1993). Thus, NMDA distribution is most likely not homogeneous but specific.

Such a voltage-dependent excitatory input can implement a multiplicative-like interaction: while the EPSP produced by a single NMDA synapse might not be strong enough to allow current to flow through the associated channels, two or more simultaneous active NMDA inputs could depolarize the potential sufficiently to relieve the Mg^{2+} mediated blockage and lead to a much larger depolarization (Fig. 4.8; Koch, 1987). Motivated by the possibility that such interactions can instantiate a specific class of computations underlying certain forms of learning, Mel (1992, 1993, 1994; Mel and Koch, 1990; see also Brown, Zador, Mainen and Claiborne, 1992) initiated a detailed biophysical investigation of synaptic integration in the dendritic tree of cortical pyramidal cells on the basis of three different mechanisms: NMDA receptors, calcium and sodium-mediated active dendritic membrane conductances. In this chapter we focus on the interaction occurring in a passive dendritic tree among NMDA synapses, deferring the more complex set of events that can occur in a dendritic tree with voltage-dependent conductances to section 19.3.4.

The basic question Mel addresses is the following: what is the sensitivity of excitatory input to spatial clustering in the postsynaptic neuron? In particular, are spatially adjacent synapses in a passive dendritic tree more or less effective than the same number of synapses spread throughout the tree?

To answer these questions, Mel (1992) models the layer 5 pyramidal cell from cat visual cortex (reconstructed by Douglas and colleagues, 1991), with a passive dendritic tree and a cell body that contains the two basic Hodgkin and Huxley currents, I_{Na} and I_K, necessary for spike initiation (and that are described exhaustively in the following chapter). Mel randomly distributes 100 synapses in clusters of k over the entire dendritic tree, like sprinkling salt over food. Fig. 5.6 illustrates this procedure for cluster size k =1 and 7: in the first case 100 synapses are placed at random within the dendritic tree while in the second case clusters of seven synapses each (plus one cluster of two synapses) are randomly assigned to 14 locations in the tree. In the absence of any NMDA input, each synapse is located onto a dendritic spine and treated as a fast, glutamergic input of the AMPA type. In the alternative case, 90% of the postsynaptic conductance increase is of the NMDA type, using the membrane potential and time dependence of eq. 4.6 (Fig. 5.7). The NMDA-mediated synaptic current, the product of the driving potential (which decreases for increasing levels of membrane depolarization) and the conductance change (which first increases and subsequently saturates with increasing V_m), increases to about -30 mV potential, after which it decreases and reverses sign at the synaptic reversal potential of 0 mV. The remaining 10% of the synaptic conductance is of the AMPA type.

All synapses (whether belonging to the same cluster or not) are activated independently of each other at a mean rate of 100 Hz. As a measure of cell response, Mel considers the number of spikes triggered over a 100 msec period. Using the peak somatic potential or the time integral of the somatic potential (in the absence of a somatic spiking mechanism) gives results that are little different. In the passive cell with voltage-independent inputs, the somatic response following activation of 100 synapses randomly located throughout the dendritic arbor is much bigger than the response following activation of 14 clusters of 7 neighbouring synapses. Indeed, the former situation triggers 4 spikes while the latter none

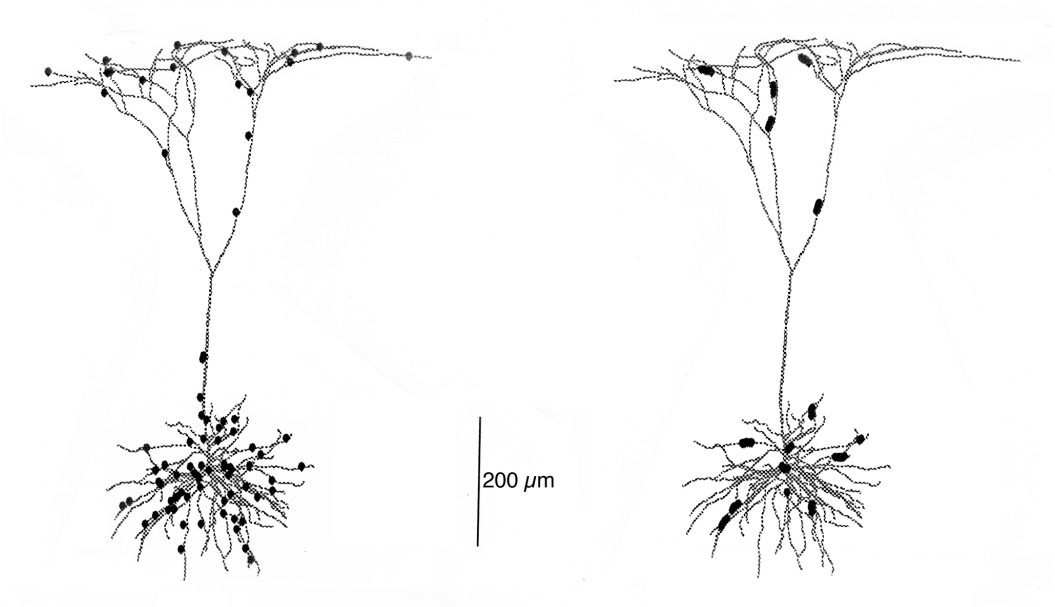

Figure 5.6: CELLULAR RESPONSE TO NON-CLUSTERED AND CLUSTERED INPUT
In the study by Mel (1992), the layer 5 pyramidal cell is festooned with 100 fast, excitatory synapses that are either spread out over 100 randomly selected individual locations (left side) or clustered at 14 randomly chosen locations of 7 synapses each (right side). In a passive dendritic tree and in the absence of NMDA input, clustered synaptic activity lead to a reduced somatic response compared to the case when synapses are dispersed. For synaptic input of the NMDA type, cooperativity exists, such that spatial clustering causes an enhanced somatic response. From B. Mel, personal communication.

(even though here the local response is larger; but, of course, fewer clusters contribute toward the somatic excitability).

If the cell's membrane is endowed with NMDA channels, it will respond selectively to patterns of stimulation in which activated synapses are spatially clustered rather than uniformly distributed across the tree (Fig. 5.7). The cell fails to spike in response to random activation of 100 NMDA "isolated" synapses to a 100 Hz input, while it fires at an effective rate of 20 Hz if the same 100 synapses are clustered in ten locations (Mel, 1993).

This preference for spatial clustering relative to a more uniform synaptic distribution for NMDA input is confirmed statistically by generating a large number (either 50 or 100) of randomized synaptic distributions of the type shown in Fig. 5.6 and averaging over the results for cluster size ranging between 1 and 15. The effect is clear and unambiguous (Fig. 5.8). Due to synaptic saturation, non-NMDA input will always be more effective when spread out in space, while the converse is true for NMDA input: as the size of the cluster is increased (and even though the number of cluster sites goes down since the total number of synapses remains fixed) the cellular response increases. For very large cluster sizes the attenuating effects of synaptic saturation begin to offset the excitatory effects of the NMDA

voltage-dependence.

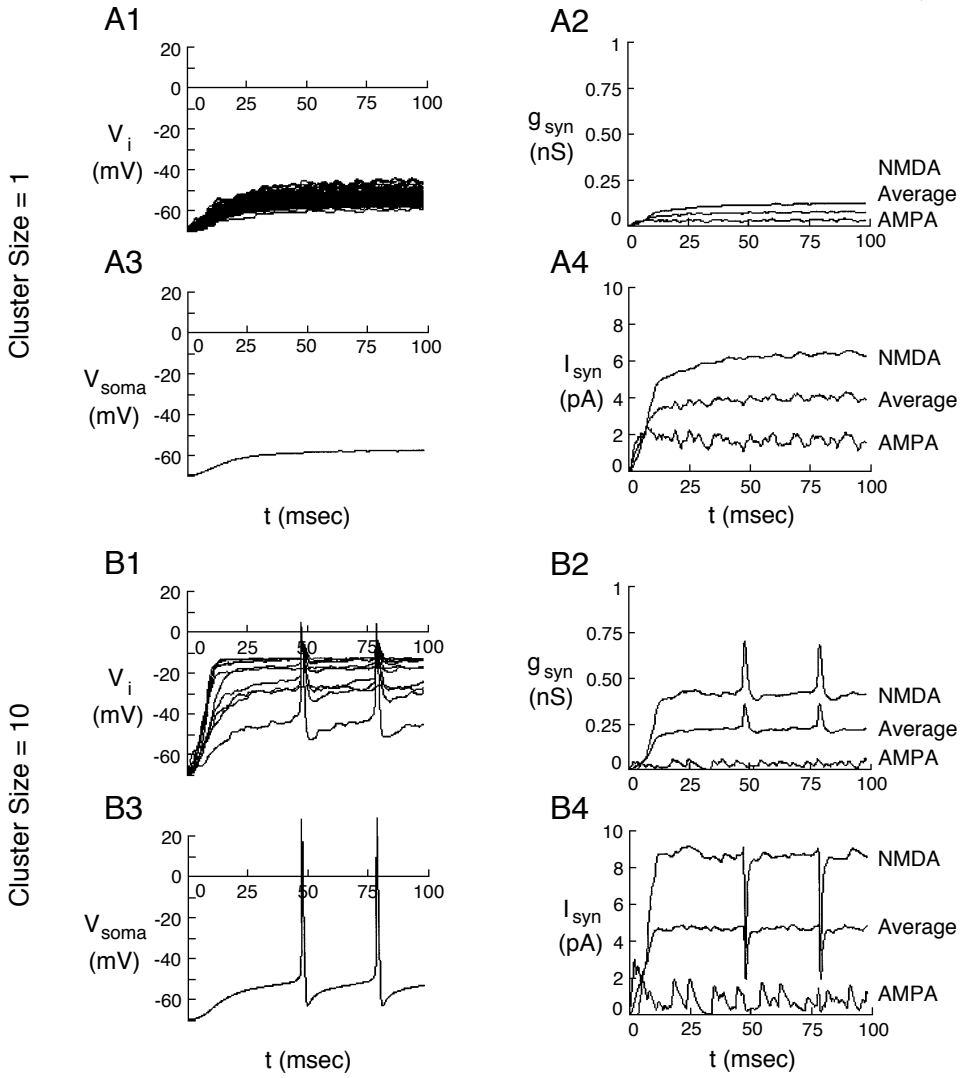

Figure 5.7: Details of the Cell's Response to NMDA Synaptic Input
Membrane potential at the synapses ($\mathbf{A}_1$, $\mathbf{B}_1$) and at the soma ($\mathbf{A}_3$, $\mathbf{B}_3$) in response to 100 uniformly distributed synapses (upper panels) and to 10 clusters of 10 synapses. 90% of the synaptic conductance change is of the NMDA type, the remainder being voltage independent. Each synapse, whether within a cluster or not, is independently activated by a Poisson process of 100 Hz rate. Because in the first case, synapses act "alone," the average synaptic conductance ($\mathbf{A}_2$) and synaptic current ($\mathbf{A}_4$) remain modest. If, however, synapses can "cooperate" due to spatial proximity the effective synaptic conductance ($\mathbf{B}_2$) and synaptic current flowing ($\mathbf{B}_4$) can be much larger, inducing the cell to fire at 20 Hz. The synaptic conductance changes scale inversely with the local input resistance, with high g_{peak} values at the soma and low ones in the distal dendritic tree. From Mel (1993).

While the exact shape of the curve in Fig. 5.8B, such as the most effective cluster size, depends on the details of the biophysical setting, the overall shape does not. Its convex shape is due to cooperativity for small cluster size and synaptic saturation for large cluster sizes (*i.e.*, the subsynaptic potential approaching the synaptic reversal potential) and is extremely robust to parameter variations (Mel, 1992).

We conclude that due to the voltage-dependency of the NMDA receptor complex, cooperativity pays off, in the sense that a cluster of adjacent synapses will lead to a larger postsynaptic response than if the synapses are randomly distributed throughout the tree. As opposed to the more demanding spatial accuracy in positioning excitation and shunting inhibition to obtain the AND-NOT effect discussed in section 5.1, cluster sensitivity does not depend on the exact positioning of synapses within a cluster. Thus, it places much less premium on development mechanisms to carefully "wire" up the synaptic architecture of the cell. Mel (1992, 1993) made no special assumptions about temporal synchronization among synaptic inputs: if input to a cluster arrives as a highly synchronized wave of excitation, it can be much more powerful than if spread out over time. In this sense, his analysis represents a worst-case scenario.

The sensitivity to spatial clumping of synaptic input is present under a broad parameter regime, in particular in the presence of calcium or sodium conductances in the dendritic tree (as we will discuss in more detail in chapter 19). Cluster sensitivity appears to represent a neurobiologically plausible mechanism to confer nonlinear, multiplicative properties to local *subunits* in the dendritic tree. Such a subunit could be more rigorously defined as a region of the dendritic tree within which synaptic interaction is strong and nonlinear, while interaction between two or more subunits would be linear (Koch *et al.*, 1982).

5.2.2 Cluster Sensitivity for Pattern Discrimination

Mel (1992) provides a illustrative example of how the nonlinear, cooperative interaction of NMDA synapses can implement a high-level computation, discriminating one pattern amongst many others.

The basic idea is straightforward: if a set of synaptic afferents coding for pattern "A" terminate in a synaptic cluster onto a particular neuron, and a large set of patterns "B" maps onto a random collection of synapses spread throughout the cell, the cell can be said to recognize or discriminate pattern "A," since activating the synaptic cluster makes the cell fire, while the cellular response to activation of the randomly distributed synapses will be negligible. This is illustrated by showing how a neuron can discriminate complex patterns, here a set of 100 black-and-white photos from a summer vacation.

The coding of the gray-scale pictures is accomplished in the following manner. Fifty randomly chosen images, designated as training set, are convolved with four oriented Gabor filters on a 64 by 64 pixel grid, resulting in a population of 16,384 orientation-selective visual units. Each one of these oriented units is assumed to make a single, all-or-none output synapse onto the layer 5 pyramidal cell in Fig. 5.6: activity of one such unit would represent the presence of a particular oriented edge at that location in the image. Out of this

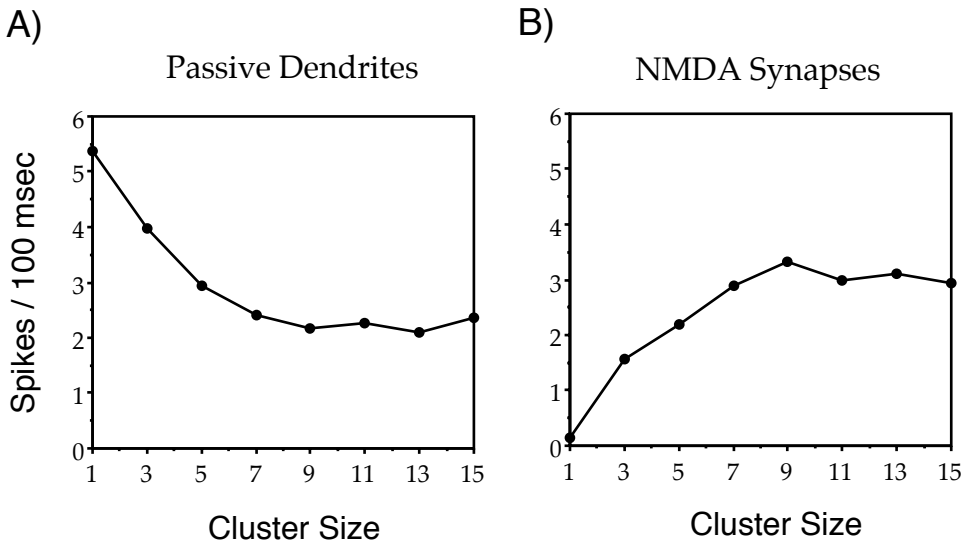

Figure 5.8: Cluster Sensitivity in a Passive Dendritic Tree
The average number of spikes within a 100 msec period using the zero NMDA **(A)** or the high NMDA **(B)** conditions as a function of cluster size. In each case, 100 synapses are placed on spines in 100/k clusters randomly distributed throughout the passive tree (with the probability density uniform in dendritic length). This procedure is repeated either 100 (for **A**) or 50 (for **B**) times for cluster sizes between 1 and 15 and the cellular response averaged. Due to the cooperativity of NMDA synapses, spatial clustering increases the postsynaptic response. This basic effect is very robust to parameter variations. Modified from Mel (1993).

---

large population, the 80 most active units are selected—the output of all other units being suppressed—and are mapped onto 10 cluster of 8 neighbouring synapses known to trigger at least one spike. This process is repeated for each of the 50 training image, except that a visual unit, once mapped onto the cell, is not remapped if it occurs in a subsequent training image. Following this "learning" procedure, the remaining unused orientation-selective units (about 12,000) are randomly mapped onto individual synaptic sites. Although a caricature of what is expected to occur in visual cortex, this procedure assures that each of the 50 images is mapped onto at most (because of the potential overlap among images) 80 clustered synapses.

As seen in Fig. 5.9, the cell responds to any one of the 50 training images with an effective spike frequency of 12.5 Hz, while the 50 randomly assigned test images fail to bring the cell above threshold. Mel (1992) also uses three sets of partially corrupted training images as input to the pyramidal cell. In the "Half/Half" stimulation paradigm, half of the vector components coding for one training image were swapped with half of the components encoding another training image. In a linear perceptron, the superposition of two training patterns cannot be distinguished from a single training pattern. In this case the cell's response is significantly reduced compared to its response to a full training pattern (by about 33%; Fig. 5.9). The same performance is seen if 20% of a training image is randomly

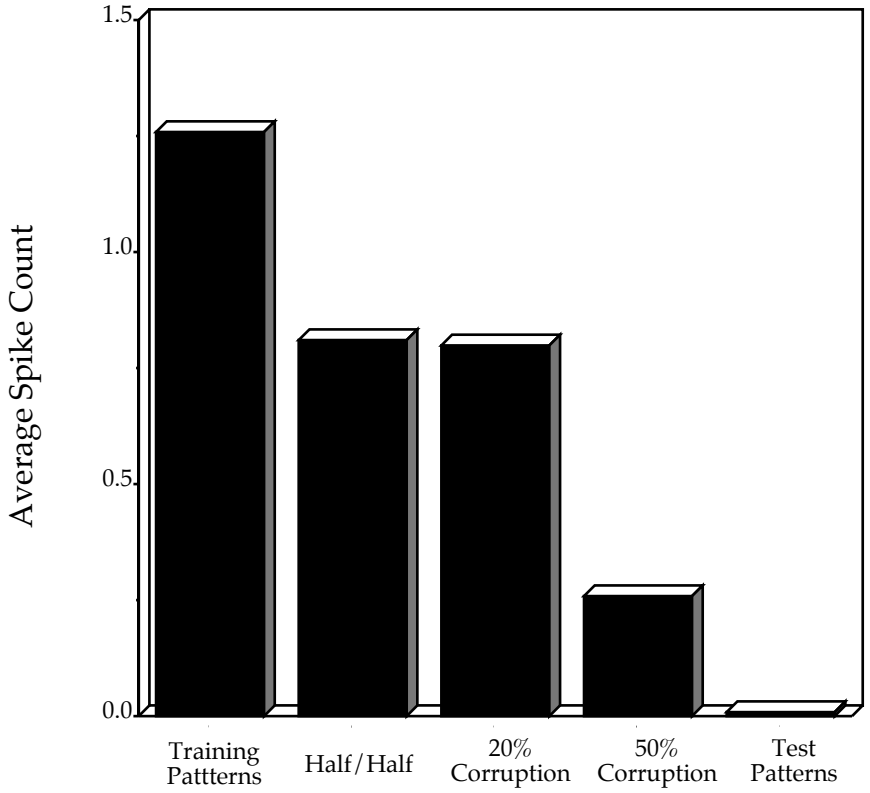

Figure 5.9: THE NMDA ENDOWED PYRAMIDAL CELL AS PATTERN DISCRIMINATOR
Average response (over a 100 msec period) of the pyramidal cell to five types of images mapped onto its synapses. The largest response is to the 50 training images and the smallest to the remaining 50 test images. In the intermediate cases, training images are partially corrupted (here indicated using a pictorial representation). In the "Half/Half" case, half of the features of one image are combined with half the features of another image. Note the significantly reduced response to the superposition of two training patterns, direct evidence of the nonlinear pattern discrimination ability of a neuron endowed with NMDA input. In the two other case, either 20% or 50 % of the image is replaced by random features. ¿From Mel (1992).

---

corrupted. If much more noise is added, the cell only responds weakly.

The performance of the pyramidal cell endowed with NMDA synapses is quite remarkable: it can be trained to respond to any one of fifty high-dimensional vectors, discriminating them from random input or vectors not beloging to the training set. The probability of misclassification is 14%, the majority of which are false negatives, that is training images not recognized as such. Given the highly dispersed three-dimensional geometry of dendritic and axonal arbors and the rich combinatorics that are possible in choosing particular spatial arrangements among 10,000 afferent synapses, the true discrimination capacity of even a single pyramidal cell could be much greater than demonstrated here (Mel, 1993, 1994; see

also Brown *et al.*, 1991a).

To what extent pyramidal cells in cortex implement such a scheme is difficult to ascertain since the detailed microanatomy of the origin of all synapses would not be sufficient to answer the question. Yet this mechanism predicts the existence of a learning rule that favors the placement of simultaneously active synapses in clusters on the dendritic tree, while uncorrelated synapses should have no specific spatial relationship to each other. Biophysical experiments involving synaptic plasticity should uncover such a rule that would lead to the clustering exploited here for computational purposes.

The degree of specificity required is less than that of the AND-NOT type of interaction discussed in the beginning of this chapter. Yet similar to the interaction between excitation and inhibition, clustering effectively fractionates the dendritic tree into many small subunits, within which nonlinear interactions take place.

5.3 Synaptic Microcircuits

Excitation and inhibition by individual synapses usually have little computational significance by themselves. It is the assembly of synapses into specific patterns of connectivity that gives rise to identifiable building blocks that can be found throughout the nervous system. Shepherd (1972, 1978) has termed such specific synaptic arrangements that have an spatial extent measured in micrometers *synaptic microcircuits*. (Fig. 5.10). Any particular neuron may have dozens or hundreds of such microcircuits. Very often they will include *dendro-dendritic* synapses, that is fast, excitatory or inhibitory chemical synapses from one dendrite of the presynaptic cell onto a dendrite from a different, postsynaptic, cell. Examples of such circuits abound in both the central nervous system of both vertebrates and invertebrates (for an excellent and detailed account of microcircuits in the mammalian brain see the monograph by Shepherd, 1990).

Well-known examples include dendro-dendritic interactions among spiking and non-spiking interneurons in sensory-motor system of the locust (Laurent and Burrows, 1989; Laurent, 1990), synaptic arrangements among the non-spiking neurons in the vertebrate retina (Dowling, 1979, 1987; Sterling, 1990; Fig. 1.5), the reciprocal dendro-dendritic inhibition occurring among the dendrites of the mitral cells and the spines of the granule cells in the mammalian olfactory bulb (Rall , Shepherd, Reese and Brightman, 1966; Rall and Shepherd, 1968; Woolf, Shepherd and Greer, 1991a,b) and the spine-triad circuit in the thalamus (Hamos, Van Horn, Raczkowski, Uhlrich and Sherman, 1985; Koch, 1985; Fig. 12.8). What characterizes these synaptic arrangements is that they involve at least one excitatory and one inhibitory synapse on a very compact spatial scale, operate at the millisecond time scale and exist in very large numbers (Shepherd, 1972, 1978; Shepherd and Koch, 1990).

Curiously, synaptic microcircuits do not appear in any significant numbers in mature cortical structures. To a good first approximation, fast excitatory and inhibitory traffic is mediated from the presynaptic axon of one cell to the postsynaptic dendrites of another cell without the involvement of higher order synaptic arrangements nor the dendro- dendritic

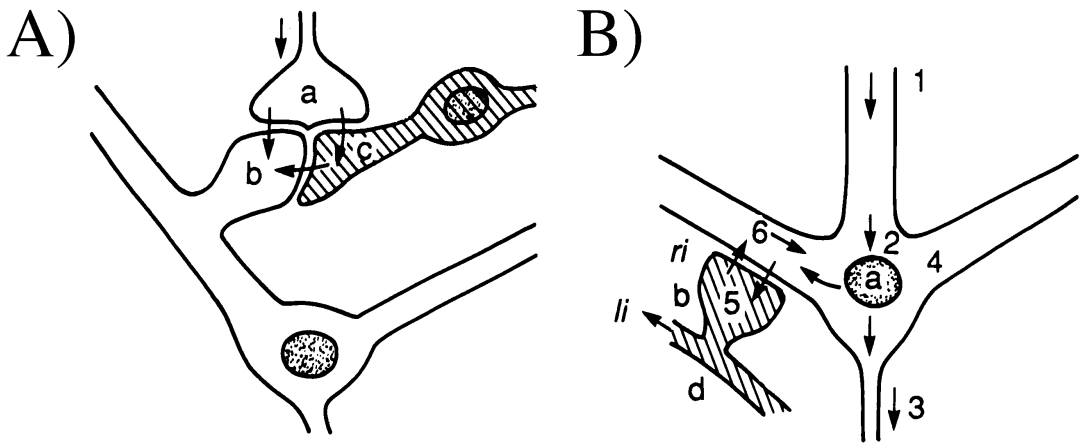

Figure 5.10: SYNAPTIC MICROCIRCUITS MEDIATING DIFFERENT TYPES OF INHIBITION
Two types of synaptic microcircuits that mediate two types of inhibition in the vertebrate nervous system. **(A)** The *spine-triade* consists of an afferent (a) making an excitatory synapse onto a dendrite or spine (b) as well as onto an interneuron (c). The interneuron in term inhibits, via a dendro-dendritic synapse, the postsynaptic neuron (b). This feedforward inhibition is common in the retina and thalamus (see section 12.3.4 and Fig. 12.8). **(B)** Recurrent inhibition is implemented by a relay cell (a) that excites an interneuron (b). This interneuron inhibits, via a dendro-dendritic synapse, the original relay cell. Dendro-dendritic reciprocal inhibition occurs between mitral and granule cells in the olfactory bulb. Such microcircuits that are specified at the micrometer level are common in structures outside cortex proper and in invertebrates. From Shepherd and Koch (1990).

---

synapses[2].

5.4 Recapitulation

The fact that a synaptic input changes the conductance in the postsynaptic membrane in series with a synaptic battery and does **not** correspond to a constant current source ultimately implies that synaptic inputs interact with each other via the membrane potential. In particular, the somatic potential in a passive tree in response to two or more inputs is **not** equal to the sum of the individual synaptic components. We explored the computational consequences of this in two cases.

The interaction between voltage-independent non-NMDA excitatory input and shunting inhibition (*i.e.* when E_i reverses close to the cell's resting membrane potential), in the subthreshold domain can mediate a veto operation that is specific in space and time: if inhibition is adjacent to the excitatory synapse or on-the-path between excitation and the

[2]It could be argued that an exception to this rule are the small fraction of dendritic spines that carry both an excitatory as well as an inhibitory synaptic profile; it is doubtful, though, whether such arrangements have a specific function (section 12.3.3).

cell body and if their time-courses overlap, inhibition can effectively suppress the effect of excitation. This implies that specific synaptic arrangements in a dendritic tree can implement logic-like AND-NOT operations, possibly one of the crucial nonlinearities underlying direction selectivity in retinal ganglion cells.

The specificity of synaptic interaction represents at the same time also its greatest weakness, in the sense that it places great demands on developmental mechanisms to precisely guide synapses and dendrites during development. A more plausible synaptic arrangement could be implemented at the level of synaptic populations: if excitatory and inhibitory synapses are co-localized onto the same part of the dendritic tree, excitatory input can always override any inhibitory influence. Conversely, if inhibition is at a different site, for instance close to the spike initiating zone, and excitation at more distal sites, then any excitatory input can always be vetoed by inhibition. These two types of synaptic placements might instantiate different kinds of suppressive behaviors: under certain conditions the threshold for initiating a reflex should be elevated (relative suppression) while under others the behavior needs to be totally abolished (absolute suppression).

If GABAergic inhibition has a reversal potential much below the membrane resting potential, as in the fly tangential interneurons, inhibition tends to act akin to a linear subtraction.

A more plausible mechanism to implement multiplicative behavior involves NMDA synapses clustered over the dendritic tree. When clusters of adjacent non-NMDA synapses are randomly sprinkled around the dendritic tree of a pyramidal cell, their activation causes a smaller cellular response then when the synapses are isolated from each other, a consequence of synaptic saturation. A very different behavior is obtained with clusters of voltage-dependent NMDA synapses. Because of their cooperative nature, clusters of 6 to 10 adjacent NMDA synapses are much more effective than the same number of synapses by themselves. A dendritic tree endowed with such synapses can be used to implement a very efficient nonlinear pattern discriminator that is robust to the presence of dendritic nonlinearities, while also serving as a plausible biophysical mechanism for multiplication required for a host of computations, such as motion, binocular disparity and tabular look-up storage.

Both case studies imply that the dendritic tree, rather than just performing a filtering operation onto the synaptic input, as suggested by linear cable theory presented in chapters 2 and 3, can be partitioned into numerous spatial subunits. Within each such subunit, synaptic inputs interact nonlinearly, while the interaction between two or more subunits is approximately linear.

Finally, we mentioned the concept of a *synaptic microcircuit*, pioneered by Shepherd (1978, 1990). These usually involve a combination of one or several excitatory and inhibitory synapses with a predilection for a specific arrangement among two or three neurons and are common in extracortical structures such as the retina, the olfactory bulb and the thalamus and in invertebrates.